JOURNAL OF ELECTROMAGNETIC ENGINEERING AND SCIENCE, VOL. 24, NO. 3, 294~304, MAY. 2024

https://doi.org/10.26866/jees.2024.3.r.230
ISSN 2671-7263 (Online) · ISSN 2671-7255 (Print)

Circularly Polarized Series Array and MIMO Application for Sub-Millimeter Wave/Terahertz Band

Thinh Tien Nguyen[1] · Dong Ho Kim[2] · Jung Han Choi[3] · Chang Won Jung[1,*]

Abstract

This article presents a compact, planar, and circularly polarized array antenna operating in the W-band (84.5–110 GHz), with all its prototypes fabricated using a low-cost, traditional, microwave printed circuit board composed of Rogers RT/duroid 5880 (ε_r = 2.2, tanδ = 0.009). The final design that was fabricated and measured was a 4 × 4 array antenna having an overall size of 9 mm × 20 mm × 0.254 mm that used series feeding to reduce its sidelobes. Measurements of the 4 × 4 patch antenna array showed approximately 6.9% 3-dB axial ratio bandwidth along with 15.2 dBi maximum right-hand circularly polarized (RHCP) antenna gain at 100 GHz. The array antenna yielded RHCP radiation characterized by a low profile, low cross-polarization levels (<–25 dB), low sidelobe levels (≤–10 dB), and high radiation efficiency (>91%). Additionally, a two-port MIMO antenna system was investigated by considering side-by-side and front-to-front configurations, both of which achieved good isolation and considerable envelope correlation coefficient and diversity gain values. Therefore, the proposed series array and MIMO antennas can be reasonable candidates for 6G applications of the sub-THz band (100–110 GHz) in ultra-high-speed wireless and satellite communication systems.

Key Words: Array Antenna, Circular Polarization, Millimeter Wave, Patch Antenna, Terahertz Band.

I. Introduction

In recent years, research on applications of the sub-millimeter wave/terahertz frequency band (0.1–10 THz) has been gaining increasing attention, providing opportunities for the discovery of several promising applications. Specifically, the sub-THz band (0.1–1 THz), which has yet to be licensed for specific usage, is expected to play a significant role in future proposals for establishing wireless links with ultrahigh data rates (>100 Gbps), excellent dependability, and capacity for low-latency communications, since this band offers a broad atmospheric transmission window along with controllable losses [1].

However, the high path and molecular absorption losses related to THz frequencies, which affect the operation of wireless links, must first be addressed. To solve this issue in THz wireless and satellite communication systems, highly directional array antenna designs are essential [2].

Several array antennas with high gain and other desirable properties in the W-band (75–110 GHz) have already been proposed in the literature, including monopulse array [3–5], Yagi-like array [6], slot array [7], and low-temperature co-fired ceramic (LTCC) array antennas [8]. However, the construction of most of these antennas not only involves a high profile and high costs, but they also use linear polarization. The perfor-

Manuscript received July 06, 2023 ; Revised August 31, 2023 ; Accepted October 18, 2023. (ID No. 20230706-125J)
[1]Graduate School of Nano IT Design Fusion, Seoul National University of Science and Technology, Seoul, Korea.
[2]Department of Smart ICT Convergence Engineering, Seoul National University of Science and Technology, Seoul, Korea.
[3]Fraunhofer Institute for Telecommunications (Heinrich-Hertz Institute), Berlin, Germany.
[*]Corresponding Author: Chang Won Jung (e-mail: changwoj@seoultech.ac.kr)

This is an Open-Access article distributed under the terms of the Creative Commons Attribution Non-Commercial License (http://creativecommons.org/licenses/by-nc/4.0) which permits unrestricted non-commercial use, distribution, and reproduction in any medium, provided the original work is properly cited.
ⓒ Copyright The Korean Institute of Electromagnetic Engineering and Science.

mance of linearly polarized antennas often deteriorates due to polarization misalignment between transmitting and receiving antennas [9]. To overcome this challenge, circularly polarized (CP) antennas have been proposed. However, their bandwidth is narrow, their radiation efficiency often drops below 75% [3], and they involve high fabrication costs [8].

Fabrication capabilities have also significantly limited sub-THz antenna designs because wavelengths in the sub-THz band are relatively small. To address this, novel fabrication methods that use 3D printing, which reduces time and manufacturing costs, have been proposed. In spite of this, the performance of sub-THz antennas could not be significantly improved [3]. For example, LTCC technology, which yields high accuracy and low loss, is widely used in antenna-in-package technology. Chips can be integrated into an LTCC substrate through wire bonding or flip-chip interconnects [8]. However, LTCC materials have high fabrication costs, which largely depend on the desired number of crafting layers, and are time-consuming for sub-THz antennas. In contrast, antennas created by machining on printed circuit boards (PCB) [10] offer the benefits of low cost, lightweight design, and ease of fabrication.

Based on the above discussion, microstrip patch antennas [11, 12] emerge as a practicable solution for use in wireless and satellite communication systems because of their low profile and considerably lower fabrication time and cost. In this context, array antenna design can also be considered extremely important. Notably, the feed network design of array antennas [13–20] uses the series-fed technique and single-fed patches to reduce sidelobe levels (SLLs) and cross-polarization, thus achieving high gain.

Additionally, in terms of avoiding problems related to high data rates, which is a desirable feature in wireless communication since it enables the accommodation of more wireless services, multiple-input-multiple-output (MIMO) technology has gained increasing attention for its unique properties that offer increased channel capacity and improved reliability [21].

II. Antenna Development Process

This section describes the process of creating two orthogonal modes of resonance as diagonal modes to yield linear polarization along the direction of the two orthogonal modes of a truncated-corner square antenna. Notably, the operating frequency band and the feed point were chosen such that the two modes could be excited in the phase quadrature, leading to the formation of CP waves on implementing the antenna [13]. Furthermore, the robust development process from the 1 × 4 array antenna to the 4 × 4 array antenna is detailed in this section.

1. Analysis of the Array Factor of 1 × 4 Array Antenna

The configuration of the array antenna is depicted in Fig. 1. Notably, the calculations of the theoretical dimensions w_p and l_p for the rectangular microstrip patch elements are provided in [13]. The substrate used for this structure is Rogers RT/duroid 5880 ($\varepsilon_r = 2.2, \tan\delta = 0.009$), with $h = 0.254$ mm.

Both the radiation patch and ground plane thicknesses were $t = 0.035$ mm. As shown in Fig. 1, the array antenna consists of four elements—the feed strip radiator and radiator positioned above the top substrate, the ground plane located beneath the bottom substrate, and two holes punched from the top to the bottom of the antenna. These holes are maintained in a fixed position between the connector, which is responsible for exciting the antenna and the PCB. Furthermore, the feedline signal head is slightly beveled to prevent contact between the antenna signal line and the connector ground. Numerical analysis of this antenna was conducted using the ANSYS High-Frequency Structure Simulator (HFSS). The design was thoroughly optimized before fabrication, the values of which are presented in Table 1. Moreover, the 1 × 4 array antenna, exhibiting a low SLL, was designed using the Dolph–Chebyshev distribution by adjusting the distance between adjoining single antenna elements. Notably, in the series-fed model of the patch array antenna, the spacing between single patches had to be optimized. Furthermore, because of the cumulative transmission characteristics of the preceding patches on the line, the transmission characteristics of the patches had to be accurately determined to achieve the desired amplitude and phase distribution of the radiating currents, along with the array. As shown in Fig. 1, the excitation amplitude of the linear microstrip array antenna is tuned using the distance between the single patches instead of the patch width. Fig. 2 clarifies the principle adhered to in this method, presenting the equivalent series circuit illustration with *N* antenna elements. The antenna elements are denoted using the radiation

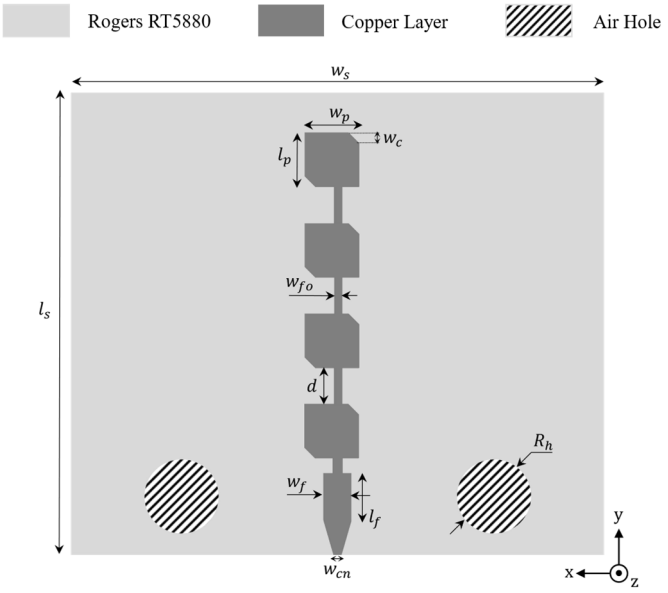

Fig. 1. Structure of the 1 × 4 array antenna.

Table 1. Optimized dimensions of the 1 × 4 array

Parameter	Value (mm)
w_p	0.91
l_p	0.81
w_c	0.175
h	0.254
d	1.11
w_{f0}	0.125
w_f	0.75
l_f	1.5
R_b	0.825
w_{cn}	0.1
w_s	9
l_s	10

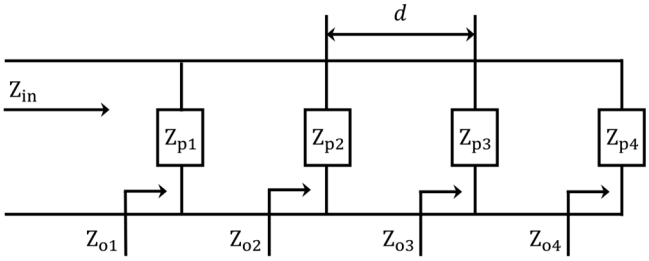

Fig. 2. Traditional structure of a 1 × 4 array antenna.

resistance Zp_i and their corresponding weights w_i, while the feedline's resistance caused by the patch elements is represented by Zo_i (i = 1, 2, …, N). The array factor (AF) can be determined using the following formula:

$$(AF)_{2N} = \sum_{i=1}^{N} w_i \cos(2nu)\ ,\ u = \frac{kdcos\theta}{2} = \frac{\pi dcos\theta}{\lambda}. \quad (1)$$

For the proposed 1 × 4 array antenna, this study realized N = 4, from which the polynomial order constant was determined as P = N – 1 = 3, while the desired theoretical SLL value was 20 dB.

$$(AF)_4 = w_1 \cos(u) + w_2 \cos(3u). \quad (2)$$

On converting the SLL value from dB into an integer, the following equation was obtained:

$$R_o = 10^{SLL/20} = 10^{20/20} = 10. \quad (3)$$

To shorten and implement the result obtained in Eq. (3), the relations of the state between the cosine functions were utilized, as follows:

$$\cos(u) = \frac{z}{z_o}, \cos(3u) = 4cos^3(u) - 3\cos(u). \quad (4)$$

With regard to the determination of the SLL value, parameter zo represents the magnitude of the SLL. Thus, the parameter z_o can be expressed as follows:

$$z_o = \cos\left(\frac{1}{P}cos^{-1}(R_o)\right) = \cos\left(\frac{1}{3}cos^{-1}(10)\right) = 1.54. \quad (5)$$

Using the equality between Eqs. (4) and (5), the above equation can be rewritten as follows:

$$(AF)_4 = (a_1 - 3a_2)\left(\frac{z}{z_o}\right) + 4a_2\left(\frac{z^3}{z_o^3}\right) = 4z^3 - 3z. \quad (6)$$

Ultimately, the AF of the linear array can be obtained using the following equation:

$$(AF)_4 = 1.736\cos(u) + \cos(3u). \quad (7)$$

Notably, the amplitude discrepancy among the radiation patch elements, which resulted in low SLLs, was found to be large. The theoretical ratio was 1:0.57, which was relatively difficult to reach due to the restricted variation range of resistance characteristics in terms of the distance of a single element. Therefore, this study realized the desired SLL values by changing the spacing between the single patches and maintaining an identical width for the radiating elements.

Furthermore, the gain of an array antenna (G_{Arr}) and that of a single antenna (G_S) can be related based on the following equation:

$$G_{Arr}(\theta,\varphi) = 2 \times (AF(\theta,\varphi))_{2N} + G_S(\theta,\varphi)\ (\text{dB}). \quad (8)$$

Therefore, using Eq. (8) at d = 0.5λ and θ = 76°, the theoretical array factor and theoretical gain of the 1 × 4 array antenna were achieved at 2 dB and 12 dBi, respectively.

As mentioned above, the spacing between the individual patches was optimized to achieve wide bandwidths for both the impedance and the 3-dB axial ratio (ARBW), while also maintaining the overall structural dimensions. To investigate this adjustment, the proposed prototype was examined by considering various values of d, as shown in Fig. 3. A significant increase in d resulted in a notable restriction of the –10 dB bandwidth, a reduction in the 3-dB ARBW, and a shift of the bandwidths toward lower frequencies. As observed in Fig. 3, the 1 × 4 array antenna with d = 0.5λ results in a –10 dB bandwidth at 80–107.5 GHz (29.3%) and a 3-dB ARBW at 99.8–102.5 GHz (2.67%), while the corresponding bandwidths with d = 0.6λ are 85–102.5 GHz (18.7%) and 97.5–99.8 GHz (2.3%), respectively. Ultimately, to obtain a wide bandwidth and improve the 3-dB ARBW, the optimal value of d was found to be 0.55λ, which achieved a –10 dB bandwidth of 83.2–105 GHz (23.2%) and a 3-dB ARBW of 98.2–102.1 GHz (3.9%).

2. Analysis of 4 × 4 Array Antenna

The 4 × 4 array antenna proposed in this study was designed

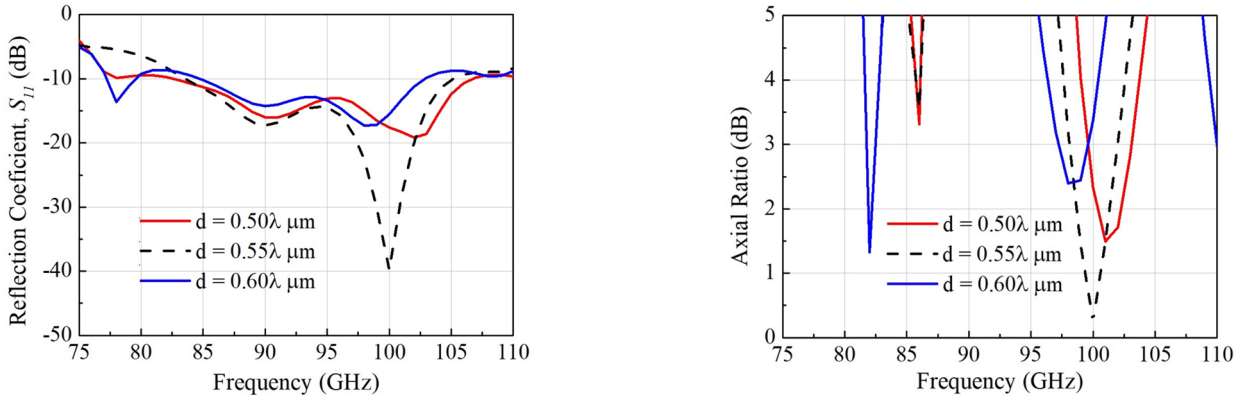

(a) (b)

Fig. 3. Simulated (a) $|S_{11}|$ and (b) axial ratio values of the 1 × 4 array antenna for various spacings between single elements (d).

to operate as a subarray for larger applications. Transitioning from the 1 × 4 array antenna described in Part 1, the proposed 4 × 4 array antenna was created using 1-to-4 power dividers. The geometry of the proposed 4 × 4 array antenna is illustrated in Fig. 4. The overall dimensions of the antenna were 9 mm × 20 mm × 0.254 mm (which is equal to $3\lambda_o \times 6.7\lambda_o \times 0.085\lambda_o$ at 100 GHz), with w_{s3} = 9 mm and l_{s3} = 20 mm. As observed in Fig. 4, the power divider bears a simple structure, using λ/4 impedance transformers of width w_{f1} = 0.085 mm, with T-junctions located where the energy separates into four identical 1 × 4 array antennas. In addition, since the radiation patches used in this structure were resonant, the input line to the patch could be matched.

Similar to the 1 × 4 array antenna, the spacing between the 1

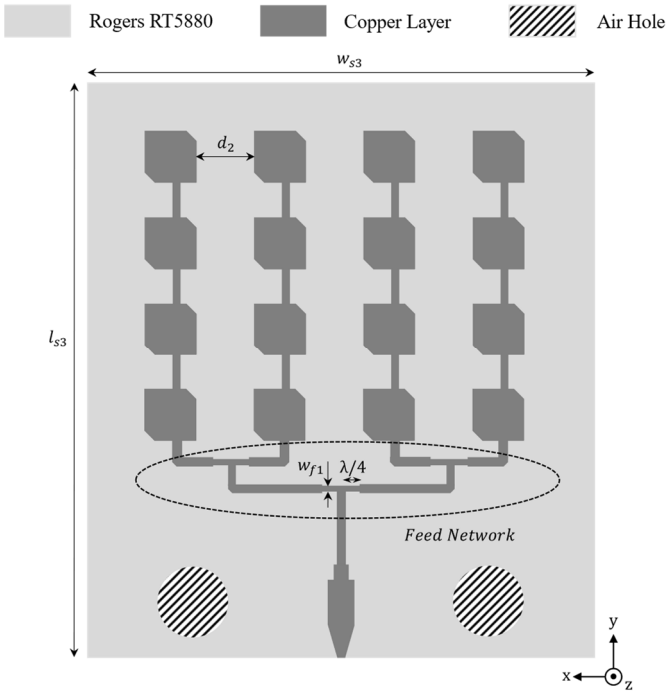

Fig. 4. Structure of the proposed 4 × 4 array antenna.

× 4 array patches (d_2) was analyzed to choose a suitable value for achieving both wide impedance and 3-dB ARBW while retaining the configuration of the 1 × 4 array antenna. As a result, the proposed antenna was investigated by testing various values of d_2, the results of which are shown in Fig. 5. When the value of d_2 was increased to the threshold value, both the -10 dB impedance and 3-dB ARBW became slightly narrow and shifted to lower frequencies. Therefore, considering the results presented in Fig. 5, to ensure both wide -10 dB impedance and 3-dB ARBW, the optimal value of d_2 was found to be 0.6λ, which yielded corresponding bandwidths of 87.5–110 GHz (22.8%) and 98.3–104.8 GHz (6.5%).

Furthermore, to understand the generation of right-hand CP (RHCP) by the proposed antenna, changes in the surface current on top of the patch change at different phases were considered. First, as shown in Fig. 6, the current is displaced in the vertical direction at the 0° phase. In contrast, at the 90° phase, the current displaces in the opposite direction. This indicates that the current moves counterclockwise as the phase values increase, thus creating the RHCP wave [9]. In addition, it was observed that the current flow through each patch element gradually changed from the vertical to the horizontal direction at phase 0°. This confirms that the AR values at 100 GHz were mainly caused by the patch.

III. Measurement and Discussion

Fig. 7 shows a photograph of the antennas under test (AUTs) in a microwave anechoic chamber along with a magnified view of the proposed antennas fabricated using a machining process on the PCB. To assess radiation performance, a sub-THz planar far-field measuring setup was employed. The setup included a frequency extender (Oleson Microwave Labs. V10VNA2-T/R) in conjunction with a vector network analyzer (Agilent E8364B) to establish a Tx antenna system, as depicted in Fig. 7.

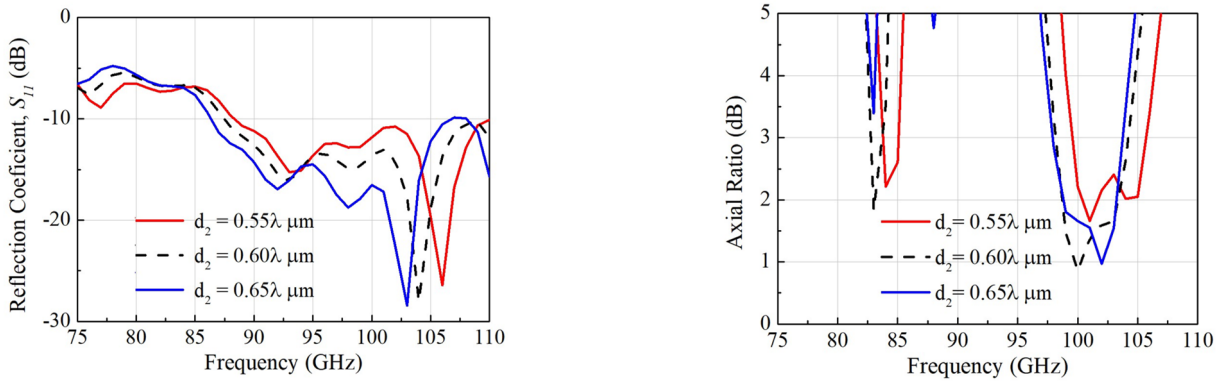

(a) (b)

Fig. 5. Simulated (a) $|S_{11}|$ and (b) axial ratio values of the proposed 4 × 4 array antenna for various spacings between single patches (d_2).

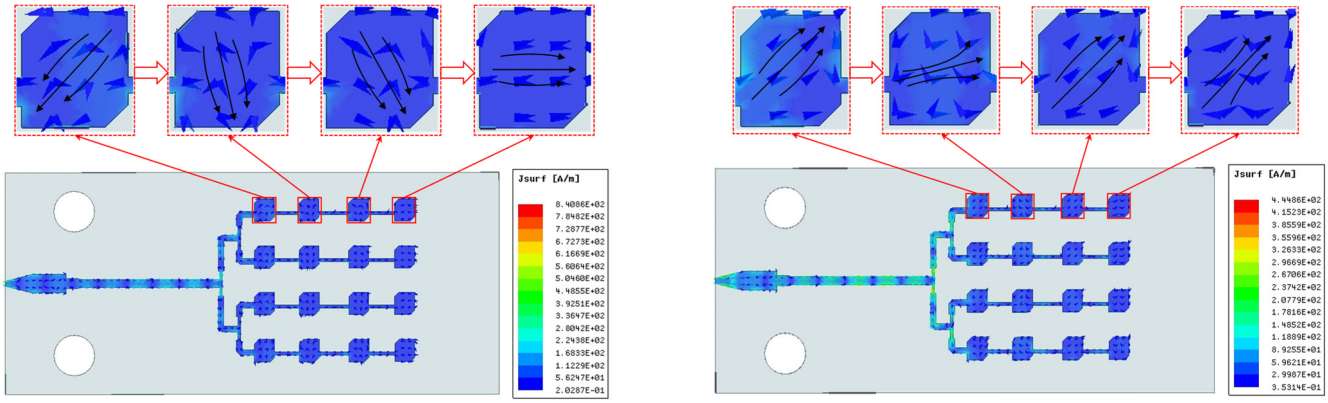

(a) (b)

Fig. 6. Current distributions on top of the patch for different phases at 100 GHz: (a) 0° and (b) 90°.

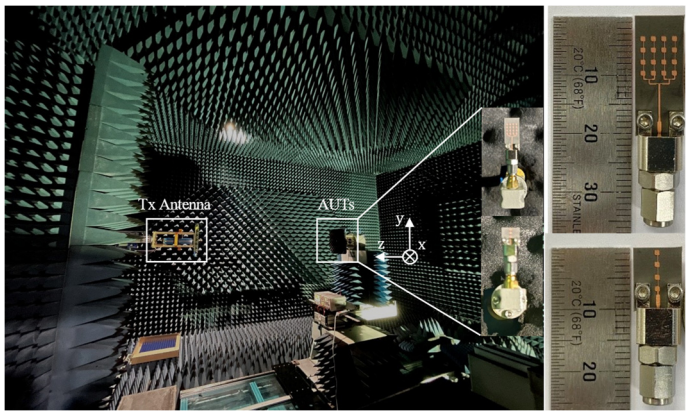

Fig. 7. Photograph of AUTs in a microwave anechoic chamber (left) and fabricated antennas (right).

The simulated and measured reflection coefficients of the 1 × 4 array antenna and the 4 × 4 array antenna are plotted in Fig. 8. Fig. 8(a) shows that the measured impedance bandwidth of the 1 × 4 array antenna at $|S_{11}| < -10$ dB is 82.5–109 GHz (27.4%), whereas the simulated -10 dB impedance bandwidth is 83.2–105 GHz (23.2%). Meanwhile, the proposed 4 × 4 array antenna exhibits a measured –10 dB impedance bandwidth of 84.5–110 GHz (26.2%), while its simulated -10 dB impedance bandwidth is 87.5–110 GHz (22.8%), as shown in Fig. 8(b). Therefore, good agreement between the simulated and measured results was achieved. Although the measured results were slightly different from the simulated values, these deviations were primarily caused by the connection between the waveguide-to-coax adapter and the feedline of the antenna.

The measured and simulated normalized radiation patterns of the fabricated antennas at 100 GHz are depicted in Fig. 9. The measured radiation pattern exhibited RHCP along with a high front-to-back ratio (F/B) and broad high-power beamwidths (HPBWs) in the *x*–*z* and *y*–*z* planes. Furthermore, the measured cross-polarization levels were more than 20 dB below the main beam in the broadside direction at 100 GHz. In particular, the measured F/Bs were 25 dB and 34 dB, while the corresponding simulated values were 25.3 dB and 33.7 dB for both planes at 100 GHz, respectively. The HPBW simulated results approximated the measured results, which were slightly displaced at ±10 and ±1.50 for the *x*–*z* and *y*–*z* planes, respec-

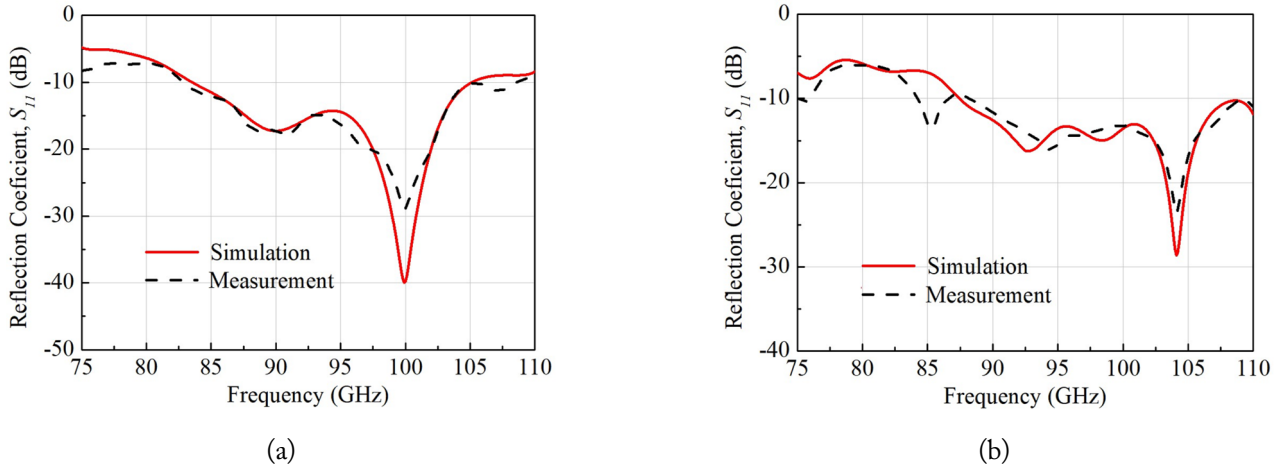

Fig. 8. Simulation and measurement of $|S_{11}|$ values of the proposed antennas: (a) 1 × 4 array antenna and (b) 4 × 4 array antenna.

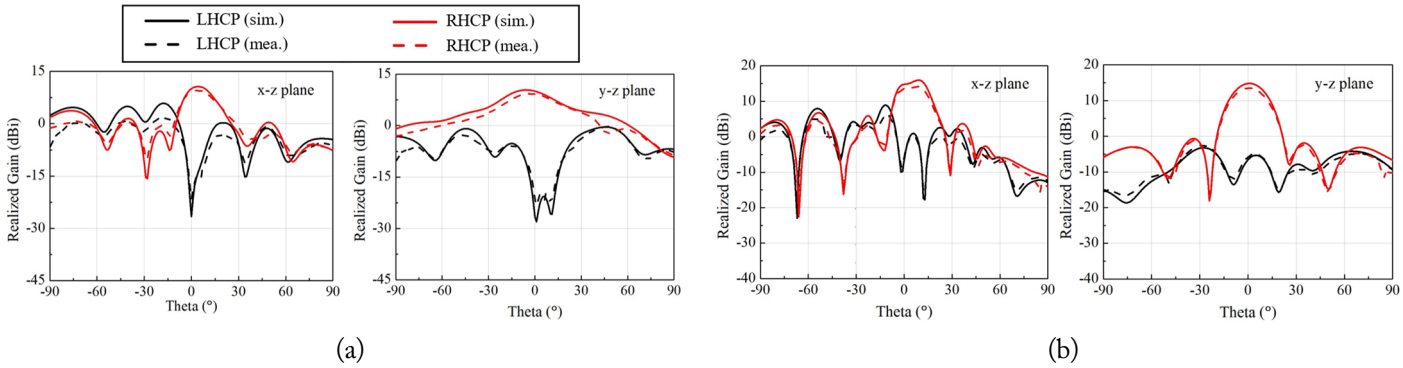

Fig. 9. Simulation and measurement results of the radiation pattern at 100 GHz for the (a) 1 × 4 array antenna and (b) 4 × 4 array antenna.

tively. With regard to the sidelobes, the measured SLL results differed only slightly from the simulated and theoretical SSL results. Notably, the SLL values of the 4 × 4 array antenna were relatively good (≤-10 dB). The values of the specific parameters are mentioned in detail in Table 2.

The measurement and simulation results for the 1 × 4 array and 4 × 4 array antennas are provided in Fig. 10. For the antenna prototypes fabricated in this study—the 1 × 4 array and 4 × 4 array antennas—the measured 3-dB ARBWs were 97.7–102.1 GHz (4.4%) and 98.2–105.1 GHz (6.9%), whereas the simulated 3-dB ARBW were 98.2–102.1 GHz (3.9%) and 98.3–104.8 GHz (6.5%), respectively. Fig. 10 presents a comparison of the simulated and measured broadside gain values of the proposed antennas. The measured results show peak RHCP gains of 10.6 and 15.2 dBi, while the simulation results exhibit peak RHCP gains of 11.1 dBi, and 16 dBi for the 1 × 4 array and 4 × 4 array antennas, respectively.

Notably, the measured values exhibited slight discrepancies compared to the simulated and theoretical ones. These could be attributed to the precision of the fabrication process, unstable test fixture connection, part loss resulting from the thickness of the substrate that could have increased the loss caused by the antenna surface waves, and an unstable chamber environment.

Table 2 compares the principal characteristics of the proposed antenna with those of various recent sub-THz arrays operating in the W-band. Compared to previous works that fabricated antennas using a 3D printing process [3], the proposed antenna used a single layer and yielded significant improvements in radiation efficiency, HPBW, impedance, and 3-dB ARBW. For an antenna composed entirely of metal and fabricated using a machining process [4], the proposed antenna offers the advantages of a compact size, sufficient CP waves, and a significant improvement in HPBW and efficiency. Moreover, in contrast to the LTCC process, the proposed antenna bears a simple structure while also offering improvements in HPBW and impedance bandwidth, as well as a reduction in fabrication and material costs [8]. Although several antenna prototypes have been fabricated on PCB material by employing machining processes [5–7], the significance of the proposed array antenna lies in the fact that it obtained CP radiation and extended both the 3-dB AR and –10 dB impedance bandwidths. Furthermore, the measurement results demonstrate that the machining process on PCB not only reduced fabrication time and cost but also achieved high precision in fabrication.

Table 2. Comparison of the performance of recent antennas and proposed antennas operating in the W-band

Study	Size (λ_o^3)	−10 dB BW[a)]	Pol./3-dB ARBW (%)	Peak gain (dBi)	Rad. efficiency (%)	# of elements	H-plane		E-plane		Ant. type	Fabrication technique
							SLL (dB)	HPBW (°)	SLL (dB)	HPBW (°)		
Tamayo-Dominguez et al. [3]	47×18.8×1.5	0.83% (93.2−94.8)	CP/0.83	27.8	70	−	−14	4	−15	5	Monopulse array	3D printing
Vosoogh et al. [4]	18.3×18.8×3	21.05% (85−105)	LP/−	30.5	70	16×16	−21	6	−16	4	Monopulse array	Machining
Cheng et al. [5]	41×39×0.16	3.2% (93−96)	LP/−	25.7	16.3	32×32	−8.3	3.23	−11.5	2.77	Monopulse array	PCB + Machining
Ghassemi et al. [6]	6.7×10×0.12	7.5% (94.2−101.8)	LP/−	18	90	4×4	−14	−	−11	−	Yagi-like array	PCB + Machining
Cheng et al. [7]	2.9×3.7×0.02	10.7% (75.9−84.5)	LP/−	11.1	38	4×4	−24	28	−13	20	Slot array	PCB + Machining
Cao et al. [8]	7.1×7.6×0.85	12.76% (88−100)	CP/10.1	22.8	N/A	8×8	−11	9	−11	12	LTCC array	LTCC
This work												
1×4 array	3×3.3×0.085	27.4% (82.5−109)	CP/4.4	10.6	92	1×4	−7	19	−17.3	36	Patch array	PCB + Machining
4×4 array	3×6.7×0.085	26.2% (84.5−110)	CP/6.9	15.2	91.5	4×4	−10	20	−15.6	21	Patch array	PCB + Machining

LP=linear polarization, CP=circular polarization.

[a)]The number in parenthesis indicates the frequency range (GHz).

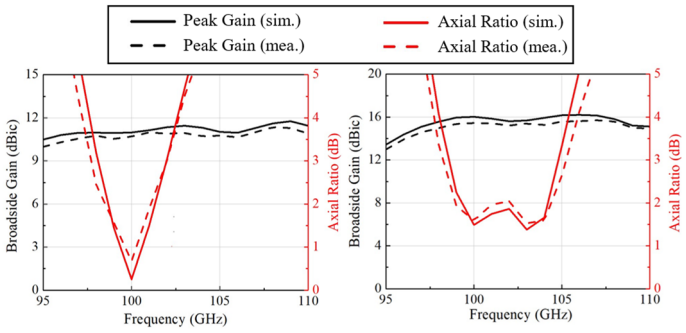

Fig. 10. Simulation and measurement results of the axial ratio and broadside gain values of the proposed antennas: (a) 1 × 4 array antenna and (b) 4 × 4 array antenna.

IV. MIMO Antenna Setup

This section demonstrates the experiments conducted using MIMO antenna system configurations in the W-band. The arrangement of the two antennas depicted in Fig. 11 presents an orthogonal configuration along with a spacing *dc*. This orthogonal arrangement enabled polarization diversity and provided a means to minimize mutual coupling between distinct antenna components, thus eliminating the need for complex decoupling structures. Simulations of both the side-by-side and front-to-front configurations of the MIMO antenna were conducted. The total dimension of the board for both configurations was L_{MIMO} × W_{MIMO}, which was equal to 20 mm × 20.5 mm and 38.2 mm × 9 mm, respectively.

Figs. 12 and 13 show the effects of the antenna element separation for both configurations by examining the impact of *dc* on antenna performance. On increasing *dc* from 4 mm to 6 mm, an enhancement in the isolation between elements was observed. Consequently, the optimal *dc* was determined to be 5 mm, which achieved a consistent reflection coefficient and favorable mutual coupling (<25 dB). This was established based on the experimental results obtained using the optimized *dc* value, which were consistent with the simulation results.

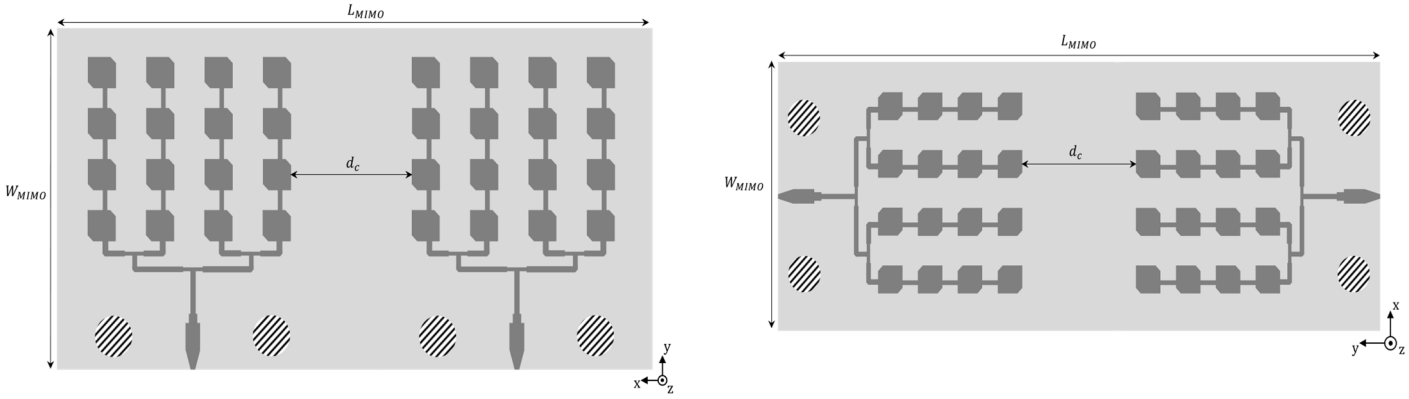

Fig. 11. Structure of the two-port MIMO antenna prototype for two distinct configurations: (a) side-by-side and (b) front-to-front.

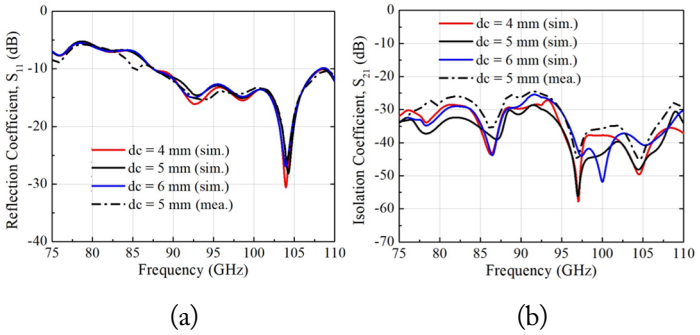

Fig. 12. Simulation and measurement result of the two-port MIMO antenna for the side-by-side configuration: (a) $|S_{11}|$ and (b) $|S_{21}|$.

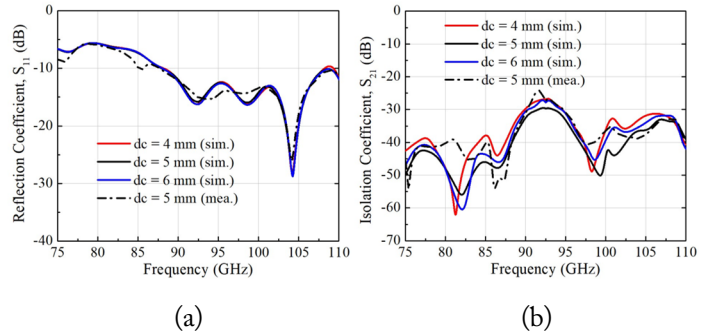

Fig. 13. Simulation and measurement result of the two-port MIMO antenna for the front-to-front configuration: (a) $|S_{11}|$ and (b) $|S_{21}|$.

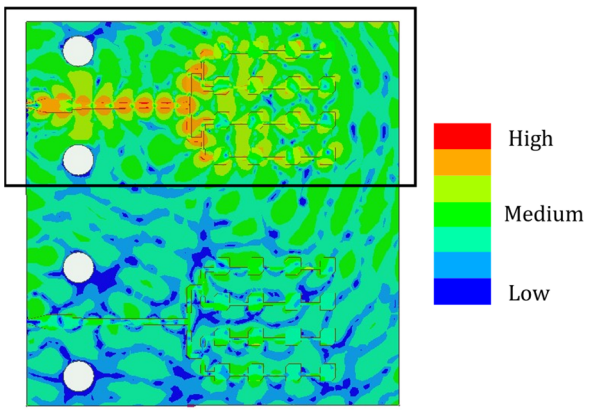

Fig. 14. Simulated E-field of the two-port MIMO antenna system for side-by-side configuration at 100 GHz.

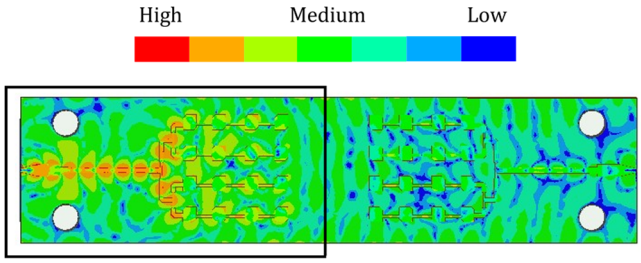

Fig. 15. Simulated E-field of the two-port MIMO antenna system for front-to-front configuration at 100 GHz.

Simulations of the E-field for the two ports of the MIMO antenna system are presented in Figs. 14 and 15. At 100 GHz, the E-field magnitude of the side-by-side configuration is observed as having collected around the patch elements and the notch of the feedline.

This indicates that all the elements in the antenna serve as radiation sources, resembling the front-to-front configuration. Furthermore, the field is primarily concentrated around the operated port with minimal E-field propagation to other ports, thereby affirming the high level of isolation between ports.

Fig. 16 plots the results of the simulated and measured radiation patterns for both configurations at 100 GHz on arranging for antenna excitation at port 1 while simultaneously closing port 2 using a 50-load. The antenna pattern achieves a pencil pattern, while the radiation pattern of the MIMO antenna seems to change insignificantly compared to the proposed antenna. In particular, the measured performance achieves a peak gain of 14.8 dBi, while maintaining low SLLs (<-10 dB) and low cross-polarization (<-20 dB).

The diversity performance of the proposed MIMO antenna was examined by utilizing diverse performance metrics, including the envelope correlation coefficient (ECC) and diversity

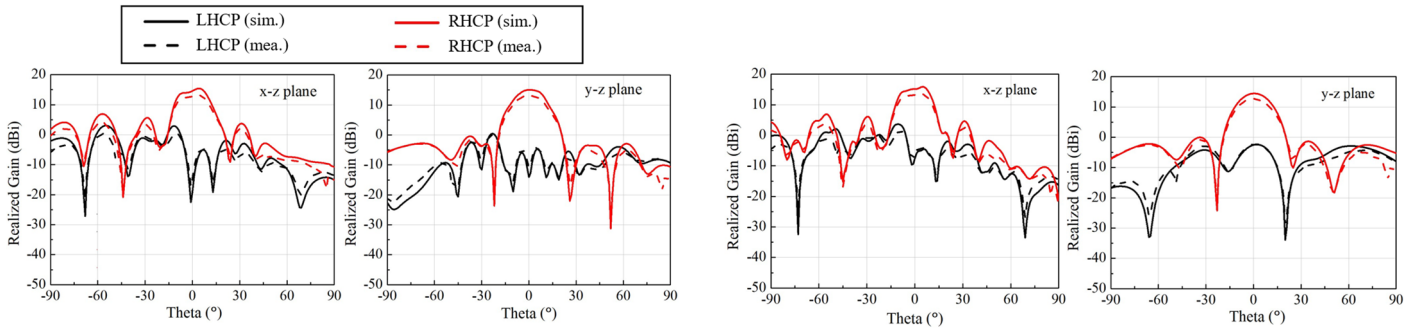

(a) (b)

Fig. 16. Simulated and measured radiation patterns of the proposed two-port MIMO antenna at 100 GHz for both configurations: (a) side-by-side and (b) front-to-front.

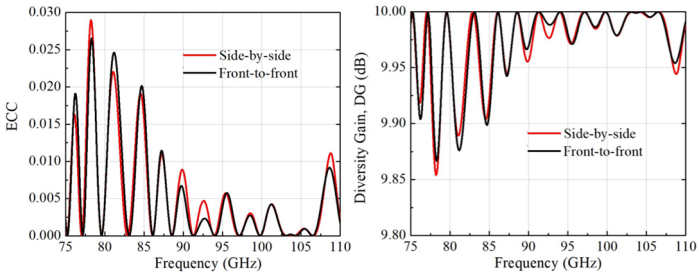

(a) (b)

Fig. 17. Measured ECC and DG of the proposed two-port MIMO antenna for both configurations: (a) side-by-side and (b) front-to-front.

gain (DG). The ECC holds great importance in MIMO systems, as it quantifies the independence of antenna elements based on their characteristics. By employing the equation noted below, the ECC characteristics of each antenna element were derived by drawing on the complex simulated results [22]:

$$ECC = \frac{|S_{mm}^{*}S_{mn} + S_{mm}^{*}S_{nn}|}{(1-|S_{mm}|^2-|S_{mn}|^2)-(|S_{nm}|^2-|S_{nn}|^2)^{*}}. \quad (9)$$

Fig. 17(a) illustrates the measured ECC results for the proposed two-port MIMO antenna, considering both scenarios. The simulations indicate ECC values below 0.0001 at 100 GHz.

To evaluate MIMO performance, the ECC and DG can be coupled using Eq. (10) [23], as noted below:

$$DG = 10 * \sqrt{1-|ECC|}. \quad (10)$$

The results of the measured DG for both configurations are shown in Fig. 17(b) in terms of the frequency of the proposed MIMO antenna. The DG value is approximately 9.99 at 100 GHz, exhibiting excellent performance for both configurations.

V. Conclusion

This work presents a compact, wide impedance bandwidth, and high-gain array antenna for the W-band. A sequential evolution from a 1 × 4 array antenna to a 4 × 4 array antenna was carried out. The 4 × 4 array antenna, with an overall size of 9 mm × 20 mm × 0.254 mm (approximately $3\lambda_o \times 6.7\lambda_o \times 0.085\lambda_o$ at 100 GHz), yielded a measured -10 dB bandwidth of 84.5–110 GHz (26.2%) and SLL peaks as low as -16 dB. The numerical and measurement results were found to be in feasible agreement. In addition, this is the first study to investigate configurations of the two-port MIMO antenna system for the W-band. Based on its superior characteristics, including a low profile, planar structure, wide operating bandwidth, stable RHCP radiation, low cross-polarization (<-25 dB), low SLLs (<-10 dB), and high radiation efficiency (>91%), and a reasonable fabrication method, the proposed 4 × 4 array and MIMO antennas can be considered appropriate candidates for 6G applications of the sub-THz band (100–110 GHz) in wireless and satellite communication systems.

This study was supported by the Research Program funded by the Seoul National University of Science and Technology.

References

[1] T. S. Rappaport, Y. Xing, O. Kanhere, S. Ju, A. Madanayake, S. Mandal, A. Alkhateeb, and G. C. Trichopoulos, "Wireless communications and applications above 100 GHz: Opportunities and challenges for 6G and beyond," *IEEE Access*, vol. 7, pp. 78729-78757, 2019. https://doi.org/10.1109/ACCESS.2019.2921522

[2] Y. He, Y. Chen, L. Zhang, S. W. Wong, and Z. N. Chen, "An overview of terahertz antennas," *China Communications*, vol. 17, no. 7, pp. 124-165, 2020. https://doi.org/10.23919/J.CC.2020.07.011

[3] A. Tamayo-Dominguez, J. M. Fernandez-Gonzalez, and M. Sierra-Castaner, "Monopulse radial line slot array antenna fed by a 3-D-printed cavity-ended modified butler matrix based on gap waveguide at 94 GHz," *IEEE Transactions on*

Antennas and Propagation, vol. 69, no. 8, pp. 4558-4568, 2021. https://doi.org/10.1109/TAP.2021.3060045

[4] A. Vosoogh, A. Haddadi, A. U. Zaman, J. Yang, H. Zirath, and A. A. Kishk, "W-band low-profile monopulse slot array antenna based on gap waveguide corporate-feed network," *IEEE Transactions on Antennas and Propagation*, vol. 66, no. 12, pp. 6997-7009, 2018. https://doi.org/10.1109/ TAP.2018.2874427

[5] Y. J. Cheng, W. Hong, and K. Wu, "94 GHz substrate integrated monopulse antenna array," *IEEE Transactions on Antennas and Propagation*, vol. 60, no. 1, pp. 121-129, 2012. https://doi.org/10.1109/TAP.2011.2167945

[6] N. Ghassemi, K. Wu, S. Claude, X. Zhang, and J. Bornemann, "Low-cost and high-efficient W-band substrate integrated waveguide antenna array made of printed circuit board process," *IEEE Transactions on Antennas and Propagation*, vol. 60, no. 3, pp. 1648-1653, 2012. https://doi.org/10.1109/TAP.2011.2180346

[7] S. Cheng, H. Yousef, and H. Kratz, "79 GHz slot antennas based on substrate integrated waveguides (SIW) in a flexible printed circuit board," *IEEE Transactions on Antennas and Propagation*, vol. 57, no. 1, pp. 64-71, 2009. https://doi.org/10.1109/TAP.2008.2009708

[8] B. Cao, Y. Shi, and W. Feng, "W-band LTCC circularly polarized antenna array with mixed U-type substrate integrated waveguide and ridge gap waveguide feeding networks," *IEEE Antennas and Wireless Propagation Letters*, vol. 18, no. 11, pp. 2399-2403, 2019. https://doi.org/10.1109/LAWP.2019.2917774

[9] S. S. Gao, Q. Luo, and F. Zhu, *Circularly Polarized Antennas*. Chichester, UK: John Wiley & Sons, 2014.

[10] I. Papapolymerou, R. F. Drayton, and L. P. Katehi, "Micromachined patch antennas," *IEEE Transactions on Antennas and Propagation*, vol. 46, no. 2, pp. 275-283, 1998. https://doi.org/10.1109/8.660973

[11] D. M. Pozar, "Microstrip antennas," *Proceedings of the IEEE*, vol. 80, no. 1, pp. 79-91, 1992. https://doi.org/10.1109/5.119568

[12] D. K. Kong, J. Kim, D. Woo, and Y. J. Yoon, "Broadband modified proximity coupled patch antenna with cavity-backed configuration," *Journal of Electromagnetic Engineering and Science*, vol. 21, no. 1, pp. 8-14, 2021. https://doi.org/10.26866/jees.2021.21.1.8

[13] D. M. Pozar and D. H. Schaubert, *Microstrip Antenna: The Analysis and Design of Microstrip Antennas and Arrays*. New York, NY: Institute of Electrical and Electronics Engineers, 1995.

[14] B. Jones, F. Chow, and A. Seeto, "The synthesis of shaped patterns with series-fed microstrip patch arrays," *IEEE Transactions on Antennas and Propagation*, vol. 30, no. 6, pp. 1206-1212, 1982. https://doi.org/10.1109/TAP.1982.1142963

[15] Y. B. Jung, I. Yeom, and C. W. Jung, "Centre-fed series array antenna for K-/Ka-band electromagnetic sensors," *IET Microwaves, Antennas & Propagation*, vol. 6, no. 5, pp. 588-593, 2012. https://doi.org/10.1049/iet-map.2011.0355

[16] Y. B. Jung, J. H. Choi, and C. W. Jung, "Low-cost K-band patch array antenna for high-sensitivity EM sensor," *IEEE Antennas and Wireless Propagation Letters*, vol. 9, pp. 982-985, 2010. https://doi.org/10.1109/LAWP.2010.2086423

[17] V. K. Kothapudi and V. Kumar, "Compact 1×2 and 2×2 dual polarized series-fed antenna array for X-band airborne synthetic aperture radar applications," *Journal of Electromagnetic Engineering and Science*, vol. 18, no. 2, pp. 117-128, 2018. https://doi.org/10.26866/jees.2018.18.2.117

[18] M. Fairouz and M. A. Saed, "A complete system of wireless power transfer using a circularly polarized retrodirective array," *Journal of Electromagnetic Engineering and Science*, vol. 20, no. 2, pp. 139-144, 2020. https://doi.org/10.26866/jees.2020.20.2.139

[19] V. K. Kothapudi, "SFCFOS uniform and Chebyshev amplitude distribution linear array antenna for K-band applications," *Journal of Electromagnetic Engineering and Science*, vol. 19, no. 1, pp. 64-70, 2019. https://doi.org/10.26866/jees.2019.19.1.64

[20] B. R. Shookooh, A. Monajati, and H. Khodabakhshi, "Theory, design, and implementation of a new family of ultra-wideband metamaterial microstrip array antennas based on fractal and Fibonacci geometric patterns," *Journal of Electromagnetic Engineering and Science*, vol. 20, no. 1, pp. 53-63, 2020. https://doi.org/10.26866/jees.2020.20.1.53

[21] M. A. Jensen and J. W. Wallace, "A review of antennas and propagation for MIMO wireless communications," *IEEE Transactions on Antennas and Propagation*, vol. 52, no. 11, pp. 2810-2824, 2004. https://doi.org/10.1109/TAP.2004.835272

[22] M. Hussain, S. Abbas, M. Alibakhshikenari, M. Dalarsson, and F. Falcone, "Circularly polarized wideband antenna for 5G millimeter wave application," in *Proceedings of 2022 IEEE International Symposium on Antennas and Propagation and USNC-URSI Radio Science Meeting (AP-S/URSI)*, Denver, CO, USA, 2022, pp. 830-831. https://doi.org/10.1109/AP-S/USNC-URSI47032.2022.9886807

[23] N. Sghaier, A. Belkadi, I. B. Hassine, L. Latrach, and A. Gharsallah, "Millimeter-wave dual-band MIMO antennas for 5G wireless applications," *Journal of Infrared, Millimeter, and Terahertz Waves*, vol. 44, pp. 297-312, 2023. https://doi.org/10.1007/s10762-023-00914-5

Thinh Tien Nguyen
https://orcid.org/0000-0002-3166-1501

received his B.S. degree in electronics and telecommunications engineering from Hanoi University of Science and Technology (HUST), Vietnam, in 2021, and his M.S. degree in electrical engineering from the Seoul National University of Science and Technology, Seoul, South Korea, in 2023. He is currently an antenna engineer at Viettel High Tech (VHT), Hanoi, Vietnam. His current research interests include sub-THz antennas, frequency-selective surfaces, millimeter-wave applications, reflect/transmit-array antennas, and reconfigurable intelligent surfaces (RIS).

Jung Han Choi
https://orcid.org/0000-0002-2007-7238

received his B.S. and M.S. degrees in electrical engineering from Sogang University, Seoul, Korea, in 1999 and 2001, respectively, and a Dr.–Ing. degree from Technische Universität München, Munich, Germany, in 2004. From 2001 to 2004, he was a research scientist at the Institute for High-Frequency Engineering at Technische Universität München, Germany. During this time, he worked on high-speed device modeling and circuit development for high-speed optical communications. From 2005 to 2011, he worked at the Samsung Advanced Institute of Technology and the Samsung Digital Media & Communication Research Center, where he dealt with RF bio sensors, nano device modeling, and circuit design for millimeter wave applications, including 60 GHz CMOS. In 2011, he joined the Fraunhofer Institute (Heinrich-Hertz Institute), Berlin, Germany. His current research interests include active/passive device design and modeling, high-frequency circuit design, and metamaterials.

Dong Ho Kim
https://orcid.org/0000-0001-9136-8932

received his B.S. degree in electrical engineering from Yonsei University, South Korea, in 1997, and his M.S. and Ph.D. degrees in electrical engineering from the Korea Advanced Institute of Science and Technology (KAIST), South Korea, in 1999 and 2004, respectively. He worked at the 4G Wireless Technology Laboratory, Samsung Advanced Institute of Technology (SAIT), from 2004 to 2006, and the Mobile Communications Research Institute, Samsung Electronics, from 2006 to 2007. Since 2007, he has been working with the Department of Smart ICT Convergence Engineering, Seoul National University of Science and Technology (SeoulTech), South Korea. His current research interests include PHY/MAC design of 5G/6G mobile communication systems.

Chang Won Jung
https://orcid.org/0000-0002-8030-8093

received his B.S. degree in radio science and engineering from Kwangwoon University, Seoul, South Korea, in 1997, and his M.S. degree in electrical engineering from the University of Southern California, Los Angeles, CA, USA, in 2001. In 2005, he received his Ph.D. in electrical engineering and computer science from the University of California at Irvine, Irvine, CA, USA. He was a research engineer in the Wireless Communication Department, LG Information and Telecommunication, Seoul, South Korea, from 1997 to 1999. From 2005 to 2008, he was a senior research engineer at the Communication Laboratory, Samsung Advanced Institute of Technology, Suwon, South Korea. He joined Seoul National University of Science and Technology, Seoul, Korea, as a professor at the Graduate School of Nano IT Design Technology in 2008. Since 2022, he has been a professor in the Department of Semiconductor Engineering at the same institution. His current research interests include antennas for multi-mode multi-band communication systems, multifunctional reconfigurable antennas, electromagnetic interference, millimeter-wave applications, optically transparent electrodes, and wireless power transfer for energy harvesting.